

Processing Poly(3-Hexylthiophene) Interlayer with Nonhalogenated Solvents for High-Performance and Low-Cost Quantum Dot Solar Cells

Jingjing Wang, Junwei Liu,* Kangkang Zhou, Kaihu Xian, Qingchun Qi, Wenchao Zhao,* Yu Chen, and Long Ye*

Hybrid solar cells with organic semiconductors and quantum dots (QDs) have witnessed great advance in the past few years. Nevertheless, the great majority of organic and QD hybrid solar cells generally employ halogenated solvents for the processing of organic hole-transporting interlayers. Herein, the impact of solvents on the organic semiconductor material for hybrid solar cells is systematically explored. The *o*-xylene-processed polythiophene delivers a champion photovoltaic performance of 8.7%, which is the record value for QD and poly(3-hexylthiophene) (P3HT) hybrid solar cells. The morphology results reveal that P3HT films processed with *o*-XY present the moderate morphology and characteristic length scales, enabling the high photovoltaic performance. Moreover, the relationships between solvents, molecular stacking, film morphology, and photovoltaic performance are built to offer the guideline of solvents screening for these hybrid solar cells. Moreover, the great superiority of nonhalogenated solvents in fabricating high-performance optoelectronic devices with low hazards is demonstrated.

With the joint efforts, PbS QD solar cells have undergone the rapid progress of photovoltaic performance from $\approx 3\%$ to over 13% during the past decade.^[10,11] Nevertheless, conventional QD solar cells generally employ *p*-type QD hole transport materials (HTMs) via tedious solid ligand exchange, which greatly compromises their commercialization potential. To further advance the commercialization progress, organic semiconductor materials are promising candidates to replace QD HTMs and may deliver new success for QD solar cells. Over the past five years, organic HTMs have enabled the great performance advance of QD solar cells from $\approx 5\%$ to $\approx 13.5\%$,^[12–16] including P3HT,^[17] PBDB-TF,^[18] PBDTPD-HT,^[19] TIPS-TPD,^[20] etc. Our group recently developed a promising polymer, brominated polythiophene, which can enable a record photovoltaic performance of 11% of QD solar cells with polythiophene-based HTMs.^[21]

Additionally, our group proposed an aggregation-suppressed blending strategy of polymeric HTMs, which can deliver a high performance of 13% for directly synthesized QD solar cells.^[22] Recently, a diketopyrrolopyrrole-based polymer was successfully synthesized for the high-performance organic HTMs.^[23] Its high hole mobility and favorable energy level enabled a record photovoltaic performance of 13.5% and a superior fill factor (FF) of 70% for QD solar cells.

1. Introduction

Due to the promising optical and electrical properties, quantum dots (QDs) have witnessed great advance in various optoelectronic devices, including solar cells,^[1,2] light-emitting diodes,^[3,4] photodetectors,^[5,6] and lasers.^[7] Lead chalcogenide QDs exhibit the broad and tunable absorption (≈ 2000 nm) and large absorption coefficients, providing a powerful platform for building infrared optoelectronic devices,^[8,9] which is unequitable for silicon-based and other solution-based semiconductor materials.

J. Wang, J. Liu, K. Zhou, K. Xian, Q. Qi, L. Ye
School of Materials Science and Engineering
Tianjin Key Laboratory of Molecular Optoelectronic Sciences
School of Environmental Science and Engineering
Collaborative Innovation Center of Chemical Science and Engineering
Tianjin University
Tianjin 300350, China
E-mail: jwliu628@tju.edu.cn; yelong@tju.edu.cn

J. Liu, L. Ye
State Key Laboratory of Applied Optics
Changchun Institute of Optics, Fine Mechanics and Physics, Chinese
Academy of Sciences
Changchun 130033, China

W. Zhao
Co-Innovation Center of Efficient Processing and Utilization of Forest
Resources
College of Materials Science and Engineering
Nanjing Forestry University
Nanjing 210037, China
E-mail: wenchaozhao@njfu.edu.cn

Y. Chen
Institute of High Energy Physics
Chinese Academy of Sciences
Beijing 100049, China

 The ORCID identification number(s) for the author(s) of this article can be found under <https://doi.org/10.1002/solr.202200779>.

DOI: 10.1002/solr.202200779

Despite the great advance, the overwhelming majority of reports on organic HTMs generally employ halogenated solvents for solar cell processing.^[24,25] It is well established that halogen atoms will accumulate into human body and ecosystems, which may lead to the severe hazard for health and environment. Therefore, it is exceedingly urgent to find eco-friendly substitutes for toxic solvents in the processing of QD solar cells, which will greatly advance the large-scale application. Only Park group processed organic HTMs with a nonhalogenated solvent, 2-methylanisole for QD solar cells, which can only achieve a comparable photovoltaic performance with that by halogenated solvents.^[26] To the best of our knowledge, there exist no reports on the systematic investigation of the performance of organic HTMs with various solvents, which has greatly compromised the superiority of QD solar cells and led to a great gap for commercial applications.

To bridge the gap, we employed the cheapest conjugated polymer, poly(3-hexylthiophene) (P3HT), to reveal the crucial role of the solvent-dependent HTM morphology in optimizing QD/polymer hybrid solar cells and explored the use of nonhalogenated solvent processing for the devices. Six commonly used solvents were employed to process poly(3-hexylthiophene) films for QD/organic hybrid solar cells. The *o*-XY-processed P3HT enabled a champion photovoltaic performance of 8.7%, which was the highest value for QD/P3HT solar cells. Moreover, the molecular stacking and film morphology were systematically characterized via atomic force microscopy (AFM), transmission electron microscopy (TEM), and grazing incidence wide-angle X-Ray scattering (GIWAXS), which can reveal the underlying mechanism of the striking performance with *o*-XY-processed films. Last but not the least, the interaction parameter between polymer and solvents was employed to further build the guideline of solvents processing for QD/polymer hybrid solar cells.

2. Results and Discussion

The P3HT used in this work was synthesized by eco-friendly polycondensation as recently reported.^[27–29] For PbS QDs, we employed directly synthesized QD inks, which exhibited the encouraging electrical and optical properties, compared with the conventional QDs with phase conversion ligand exchange. Moreover, the directly synthesized QDs can deliver the superior photovoltaic performance and stability. With these benefits, we prepared the directly synthesized QDs according to our recent work.^[21,22] The nuclear magnetic resonance spectrum of P3HT can be found in Figure S1, Supporting Information, from which we can determine the regioregularity ($\approx 90\%$). Gel permeation chromatography was employed to characterize the molecular weight and polydispersity index of P3HT, and the results are plotted in Figure S2 and Table S1, Supporting Information.^[30] Additionally, cyclic voltammetry was employed to confirm the energy level of P3HT (Figure S3, Supporting Information), which exhibited a highest occupied molecular orbital (HOMO) energy level of ≈ 4.86 eV. Combined with the absorption results (Figure S4, Supporting Information), we can draw the energy-level diagram of QD/polythiophene heterojunction with a favorable type-II energy-level alignment (Figure S5, Supporting Information).^[31–33]

Subsequently, this work aims to build fundamental relationships between casting solvent, film morphology, and photovoltaic performance by screening six organic solvents, including three halogenated solvents (chloroform (CF), chlorobenzene (CB), and dichlorobenzene (DCB)) and three nonhalogenated solvents such as *o*-xylene (*o*-XY), tetrahydrofuran (THF), and 2-methyl-tetrahydrofuran (Me-THF), in which P3HT all exhibited excellent solubility. These solvents span from high toxicity to low toxicity. Nevertheless, film absorption results indicated that P3HT

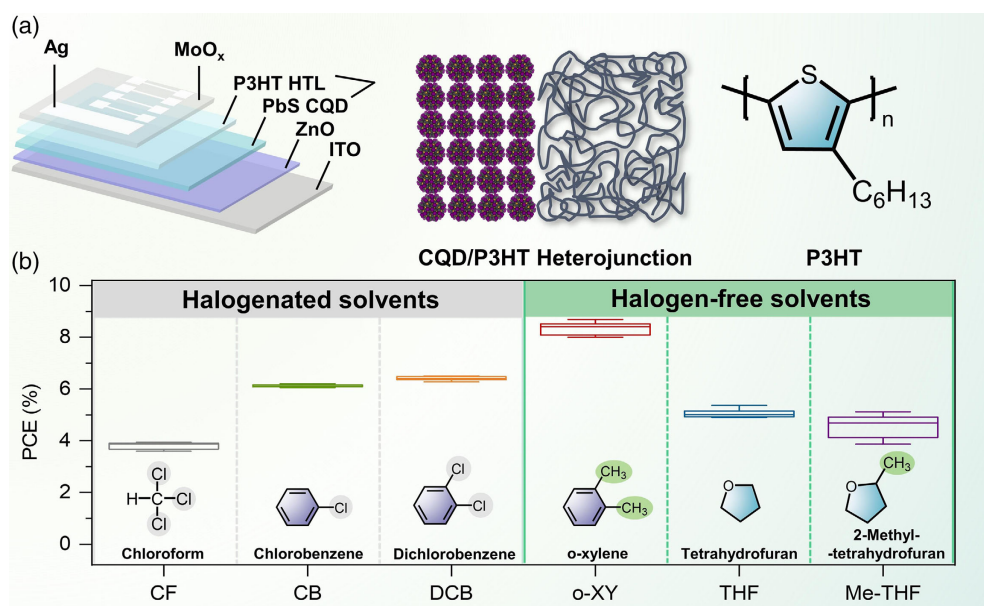


Figure 1. a) Device structure of QD/P3HT hybrid solar cells, the schematic diagram of CQD/P3HT heterojunction, and the molecular formula of P3HT. HTL denotes hole-transporting layer. b) The PCE values of QD/P3HT hybrid solar cells studied in this work and molecular formula of the different solvents for P3HT interlayers.

processed with different solvents presented distinct absorption coefficient, indicating the different aggregation of polythiophene in various solvents (Figure S6, Supporting Information). Among them, *o*-xylene-processed P3HT delivered the maximum absorption coefficient, which was favorable for the solar complementary absorption with QD active layer. Additionally, photoluminescence (PL) characterization was employed to reveal the carrier transport performance of QD/polythiophene heterojunction, and the results are plotted in Figure S7, Supporting Information. It can be clearly seen that all the heterojunction presented the single PL peak from polythiophene, indicating the efficient hole transfer from QDs to P3HT. Moreover, we also observed the distinct PL peaks of polythiophenes processed with various solvents, which also revealed the different aggregation in various solvents.^[34]

Encouraged by the different absorption and PL results, we proceeded to explore the photovoltaic performance of

QD/polythiophene hybrid solar cells with different solvents. We employed the widely used structure of ITO/ZnO/PbS QDs/polythiophenes/MoO_x/Ag (Figure 1a), which had the optimized thickness ≈ 250 and ≈ 30 nm for the PbS QD active layer and the P3HT interlayer, respectively. The *J*-*V* curves of QD/polythiophene solar cells with different solvents are shown in Figure S8, Supporting Information, from which we can observe the distinct photovoltaic performance. Specifically, the QD solar cells with CF, THF, and Me-THF exhibited the inferior power conversion efficiency (PCE) of below 5.5%, mainly stemming from the low short-circuit current density (*J*_{sc}) and FF. For CB and DCB counterparts, the moderate photovoltaic performance was achieved with a PCE of over 6%, which was comparable with the prior reports on QD/P3HT solar cells.^[17,35] Nevertheless, the open-circuit voltage (*V*_{oc}) and FF still had great improvement room, according to our recent work.^[21] We

Table 1. Photovoltaic parameters of the QD/P3HT hybrid solar cells under AM1.5 G irradiation.

Solvent for P3HT	<i>V</i> _{oc} [V]	<i>J</i> _{sc} [mA cm ⁻²]	FF [%]	PCE [%]
CF	0.556 (0.551 ± 0.004)	21.57 (21.18 ± 0.26)	32.85 (32.65 ± 0.71)	3.94 (3.81 ± 0.12)
Me-THF	0.561 (0.535 ± 0.026)	24.67 (23.83 ± 1.11)	37.03 (35.90 ± 2.56)	5.13 (4.57 ± 0.38)
THF	0.548 (0.551 ± 0.004)	24.86 (24.25 ± 0.26)	39.42 (37.84 ± 0.89)	5.37 (5.06 ± 0.14)
CB	0.564 (0.561 ± 0.002)	25.03 (24.98 ± 0.15)	43.93 (43.66 ± 0.42)	6.20 (6.12 ± 0.05)
DCB	0.546 (0.548 ± 0.007)	26.25 (25.57 ± 0.52)	45.35 (45.69 ± 0.48)	6.50 (6.40 ± 0.06)
<i>o</i> -XY	0.617 (0.596 ± 0.011)	26.65 (25.83 ± 0.42)	52.83 (54.25 ± 0.68)	8.70 (8.35 ± 0.21)

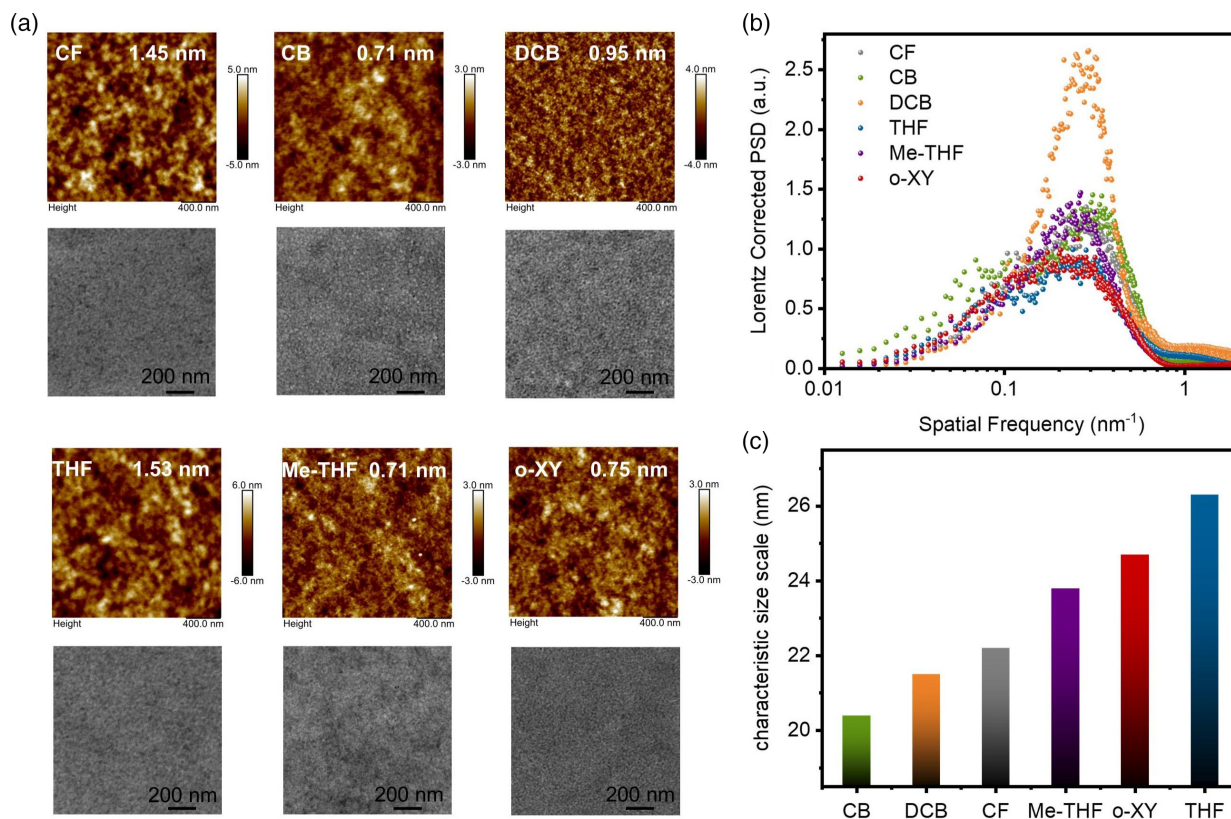


Figure 2. a) AFM and TEM images, b) PSD profiles, and c) characteristic size scales of P3HT interlayers casted from different solvents.

proceeded to investigate the performance of QD solar cells with P3HT processed by *o*-XY and observed the marked improvement of V_{oc} , J_{sc} and FF (Figure 1b and Table 1), resulting in a champion PCE of 8.7% (Figure S9, Supporting Information). More strikingly, the achieved V_{oc} of 0.62 V was the record voltage value reported to date for QD/P3HT hybrid solar cells. The significantly improved V_{oc} by *o*-XY may be explained with the recent report by Zhong et al.^[36] that different solvents may induce distinct aggregation in the vertical direction of P3HT layer, resulting in the diversity of interfacial ionization energy and less carrier recombination. Additionally, the results from the V_{oc} dependence on light intensity also exhibited low trap-assisted carrier recombination, coincident with the above discussion (Figure S10, Supporting Information).

To gain more insight into the encouraging photovoltaic performance, the surface morphology of the P3HT processed with different solvents was characterized with AFM and TEM.^[37,38] The AFM height images and TEM images are shown

in Figure 2a, and AFM phase images are plotted in Figure S11, Supporting Information, from which we can clearly observe the stark morphology difference of P3HT films processed with different solvents. The root-mean-square surface roughness (R_q) of all polythiophene films was extracted, and the films with CF and THF presented the high R_q of ≈ 1.5 nm, which was not favorable for carrier transport between QDs and P3HT, as revealed by our recent work.^[21,22] For the P3HT film processed with *o*-XY, the moderate R_q for efficient carrier transport was achieved, which resulted in the improved photovoltaic performance. Additionally, we further performed the fast Fourier transform analysis of power spectral density (PSD) profiles, which can deliver a quantitative analysis of feature sizes (Figure 2b). There exists clear difference in the characteristic length scales of P3HT films with different solvents (Figure 2c). The films processed with CB and DCB presented the small feature sizes, which can explain the inferior J_{sc} and FF of the corresponding QD/polythiophene solar cells. By contrary, the films with

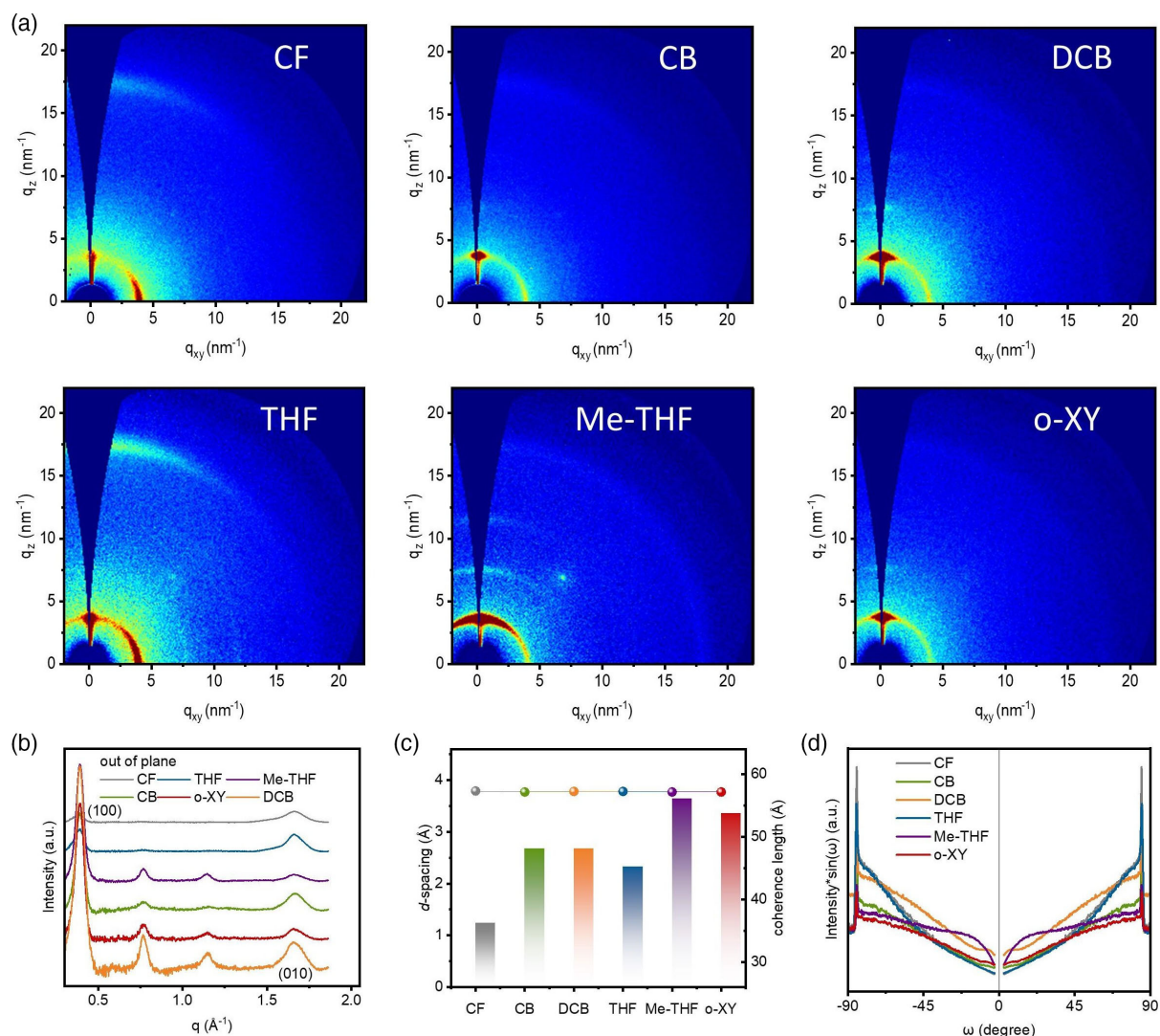


Figure 3. a) 2D GIWAXS patterns, b) 1D out of plane scattering profiles, c) the (010) d -spacings (left) and coherence lengths (right), and d) the pole figure analysis of GIWAXS patterns of P3HT interlayers casted from different solvents.

o-XY exhibited a moderate domain size, which can partially explain the efficient carrier transport and high photovoltaic performance.

To further uncover the underlying mechanism of the distinct performance of P3HT films with different solvents, GIWAXS was employed to characterize the detailed molecular stacking.^[39] The 2D diffraction patterns of P3HT films are plotted in Figure 3a, from which we can observe the noteworthy difference of the stacking and orientation with various solvents. The films with CF, THF, and Me-THF exhibited the strong (100) signals, indicating high crystallinity, which was consistent with the relatively rough morphology from AFM images. The film with *o*-XY presented the low crystallinity, which is in line with its smooth morphology and high photovoltaic performance. To deepen the understanding of molecular stacking, the 1D scattering profile analysis of P3HT films was performed, and the out-of-plane and in-plane profiles are plotted in Figure 3b and S12, Supporting Information, respectively. Accordingly, we can determine the *d*-spacing and coherence length (L_c) of P3HT films, which presented the similar *d*-spacings, but distinct L_c . The film processed with *o*-XY achieved a high L_c of 55 Å, corresponding to more ordered stacking and high photovoltaic performance (Figure 3c).^[40] Further pole figure analysis revealed that P3HT film processed by *o*-XY had the favorable face-on/edge-on ratio, which is often desired for efficient charge transport (Figure 3d). From the above discussion, we can confirm the favorable stacking and crystallinity of P3HT films processed by *o*-XY solvent, which was favorable for carrier transport and photovoltaic performance.

Based on the above encouraging results, we can further elucidate the relationships between processing solvents, molecular stacking, film morphology, and photovoltaic performance.^[41,42] We chose three representative solvents, i.e., CB, THF, and *o*-XY for the following discussion. From the GIWAXS results, we can conclude that the molecular aggregation was gradually enhanced for the films processed by CB, *o*-XY, and THF, which was consistent with the trend of characteristic length scales from AFM and TEM images (Figure 4a). The moderate aggregation of *o*-XY-processed P3HT can enable efficient carrier transport and high photovoltaic performance. To further reveal the underlying mechanism, we performed the theoretical analysis via the interaction parameter and χ between P3HT and various solvents.^[43–45] The solvent properties are shown in Table S2, Supporting Information, and the detailed calculation process can be found in Supporting Information. It is well established that small χ indicates the strong interaction between polymer and solvent, which may result in low aggregation. Interestingly, the χ values exhibited a mostly linear relationship with the corresponding characteristic length scales (Figure 4b). It can be clearly seen that *o*-XY can enable the moderate χ , therefore resulting in the favorable stacking and morphology. Consequently, a simple guideline on screening casting solvents for high-performance QD/polymer hybrid solar cells emerges. The moderate interaction parameter between polymer and solvent will result in favorable molecular stacking and film morphology, therefore delivering high photovoltaic performance (Figure 4a–d).

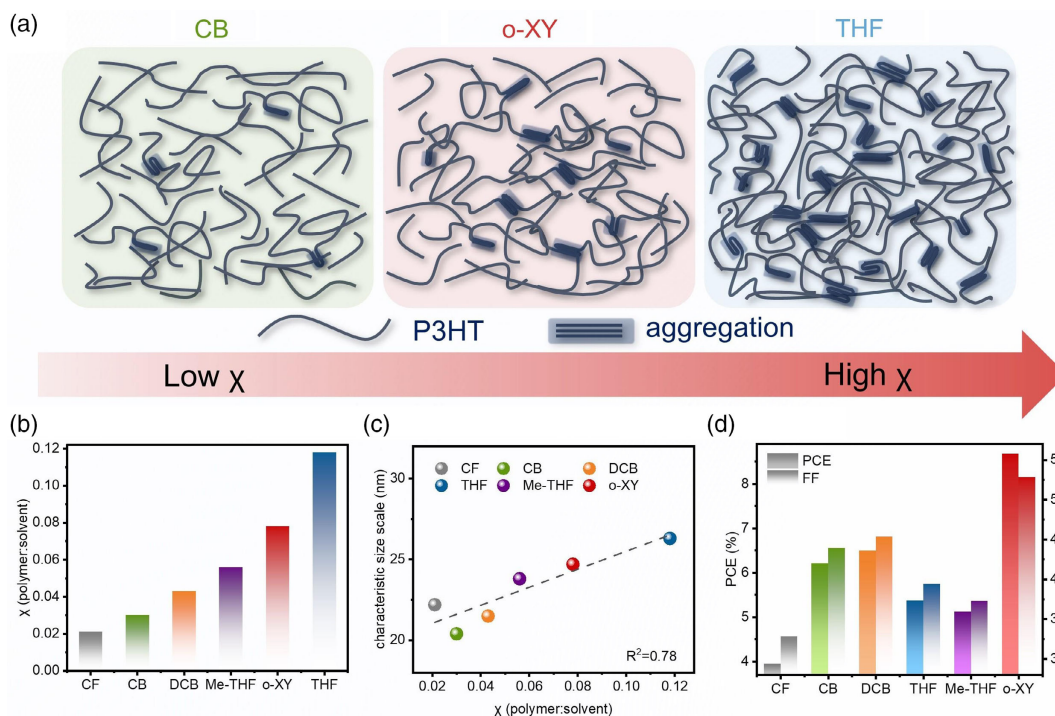


Figure 4. a) Schematic diagram of P3HT aggregation in films by using different solvents. b) The interaction parameter between P3HT and various solvents. c) The relationship between characteristic size scale and χ parameter for P3HT with different solvents. The dashed line is a linear fit. d) The PCE and FF values of the QD/P3HT hybrid solar cells.

3. Conclusions

In summary, this work revealed the profound impact of casting solvents on the hole-transporting interlayers and photovoltaic performance in QD/polythiophene hybrid solar cells. The *o*-XY-processed P3HT enabled a champion photovoltaic performance of 8.7%, the highest value for QD/P3HT solar cells. The AFM and TEM results indicated that P3HT films processed by *o*-XY presented moderate morphology and characteristic length scales, which can deliver high photovoltaic performance. Moreover, GIWAXS results also revealed the favorable stacking and crystallinity of *o*-XY-processed P3HT film. Finally, the interaction parameter between polymer and solvents was employed to further build the guideline of solvents screening for these QD/polymer solar cells. As new polythiophenes are developing rapidly,^[46–48] these nonhalogenated solvents might aid in constructing high-performance and cost-effective QD/polythiophene hybrid optoelectronic devices with low hazards for human health and environment. These explorations are under way.

4. Experimental Section

Material Synthesis: PbS QDs were synthesized in our laboratory based on the recent work. The P3HT sample ($M_w = 73.9 \text{ kg mol}^{-1}$, RR = 90%) was identical to a batch used in our prior report. All solvents were purchased from Sigma Aldrich without further purification.

Device Fabrication: The prepared PbS QDs (1100 mg mL^{-1}) were dissolved in DMF for ≈ 30 min. P3HT (6 mg mL^{-1}) were dissolved in different solvents and stirred at 55°C without any solvent additives. This work employed the widely used device structure of ITO/ZnO/PbS QDs/polythiophenes/MoO_x/Ag. ITO substrates were cleaned with detergent, deionized water, acetone, and isopropanol for 15 min, respectively. The ITO substrates were treated with ultraviolet ozone for 25 min. The ZnO sol-gel was spin-coated on ITO glass substrates at 3000 rpm for 40 s and then annealed at 200°C for 1 h. This process was repeated twice to obtain 100 nm ZnO films. Subsequently, the prepared PbS QDs solution was spin-coated on ZnO at 2000–2500 rpm for 30 s with a thickness of ≈ 250 nm and were annealed at 75°C for 15 min. Then P3HT was spin-coated on QD active layer at 2000 rpm for 30 s and then oxidized in air for 1 h. Thereafter, MoO_x/Ag (8 nm/100 nm) anode was thermally evaporated under low pressure ($< 1.5 \times 10^{-4}$ Pa).

Characterizations: Optical Properties: The absorption spectra of P3HT films casted from different solvents were measured by Shimadzu UV-3600 Plus spectrometer. Photoluminescence (PL) of PbS QDs/P3HT heterojunction was measured by the FLIM equipment consisting of the confocal optical microscope (Nanofinder FLEX2, Tokyo Instruments, Inc.). The thickness of P3HT films was measured by the surface profilometer Bruker Dektak XT.

Characterizations: Electrical Properties: The *J*–*V* curves of QD/polythiophene hybrid solar cells were measured by the Keithley 2400 source meter under the standard AM 1.5G spectrum with an AAA solar simulator (SS-F5-3A, Enli Technology Co. Ltd, Taiwan).

Characterizations: Morphology Characterizations: The AFM images of P3HT films casted from different solvents were collected by the Bruker MultiMode 8 AFM in tapping mode, and the TEM images were captured by the JEOL JEM-2100PLUS electron microscope.

Characterizations: GIWAXS Characterizations: The P3HT films with different solvents were prepared on silicon substrates to form GIWAXS samples. GIWAXS experiments were performed at the beamline 1W1A of Beijing Synchrotron Radiation Facility (BSRF). The X-Ray energy was 8 keV. The incidence angle was 0.2° , and the sample-to-detector distance was 453 mm by careful calibration.

Supporting Information

Supporting Information is available from the Wiley Online Library or from the author.

Acknowledgements

This work was supported by the Open Fund of State Key Laboratory of Applied Optics (No. SKLAO2021001A17), the Peiyang Scholar Program of Tianjin University, and the Fundamental Research Funds for the Central Universities. L.Y. also gratefully acknowledges the National Natural Science Foundation of China (No. 52073207) for support. J.L. would like to acknowledge Shanghai Tongji Gao Tingyao Environmental Protection Technology Development Foundation for support. GIWAXS data were acquired at Beijing Synchrotron Radiation Facility (BSRF), beamline 1W1A. Prof. H. Yin is appreciated for providing PL characterization.

Conflict of Interest

The authors declare no conflict of interest.

Data Availability Statement

The data that support the findings of this study are available from the corresponding author upon reasonable request.

Keywords

hybrid solar cells, interaction parameters, nonhalogenated solvents, poly(3-hexylthiophene), quantum dots

Received: August 23, 2022

Revised: September 1, 2022

Published online: September 20, 2022

- [1] J. Liu, K. Xian, L. Ye, Z. Zhou, *Adv. Mater.* **2021**, *33*, 2008115.
- [2] J. Xu, O. Voznyy, M. Liu, A. R. Kirmani, G. Walters, R. Munir, M. Abdelsamie, A. H. Proppe, A. Sarkar, F. P. García De Arquer, M. Wei, B. Sun, M. Liu, O. Ouellette, R. Quintero-Bermudez, J. Li, J. Fan, L. Quan, P. Todorovic, H. Tan, S. Hoogland, S. O. Kelley, M. Stefiik, A. Amassian, E. H. Sargent, *Nat. Nanotechnol.* **2018**, *13*, 456.
- [3] X. Li, Y. B. Zhao, F. Fan, L. Levina, M. Liu, R. Quintero-Bermudez, X. Gong, L. N. Quan, J. Fan, Z. Yang, S. Hoogland, O. Voznyy, Z. H. Lu, E. H. Sargent, *Nat. Photonics* **2018**, *12*, 159.
- [4] M. Vasilopoulou, H. P. Kim, B. S. Kim, M. Papadakis, A. E. Ximim Gavim, A. G. Macedo, W. Jose da Silva, F. K. Schneider, M. A. Mat Teridi, A. G. Coutsolelos, A. R. bin Mohd Yusoff, *Nat. Photonics* **2020**, *14*, 50.
- [5] R. Saran, R. J. Curry, *Nat. Photonics* **2016**, *10*, 81.
- [6] J. Liu, M. Gao, J. Kim, Z. Zhou, D. S. Chung, H. Yin, L. Ye, *Mater. Today* **2021**, *51*, 475.
- [7] N. Taghipour, G. L. Whitworth, A. Othonos, M. Dalmases, S. Pradhan, Y. Wang, G. Kumar, G. Konstantatos, *Adv. Mater.* **2021**, *2107532*, 2107532.
- [8] M. Liu, O. Voznyy, R. Sabatini, F. P. García De Arquer, R. Munir, A. H. Balawi, X. Lan, F. Fan, G. Walters, A. R. Kirmani, S. Hoogland, F. Laquai, A. Amassian, E. H. Sargent, *Nat. Mater.* **2017**, *16*, 258.

- [9] F. P. G. de Arquer, D. V. Talapin, V. I. Klimov, Y. Arakawa, M. Bayer, E. H. Sargent, *Science* **2021**, 373, 640.
- [10] J. Tang, X. Wang, L. Brzozowski, D. A. R. Barkhouse, R. Debnath, L. Levina, E. H. Sargent, *Adv. Mater.* **2010**, 22, 1398.
- [11] B. Sun, A. Johnston, C. Xu, M. Wei, Z. Huang, Z. Jiang, H. Zhou, Y. Gao, Y. Dong, O. Ouellette, X. Zheng, J. Liu, M. J. Choi, Y. Gao, S. W. Baek, F. Laquai, O. M. Bakr, D. Ban, O. Voznyy, F. P. G. de Arquer, E. H. Sargent, *Joule* **2020**, 4, 1542.
- [12] J. Chen, S. Zheng, D. Jia, W. Liu, A. Andruszkiewicz, C. Qin, M. Yu, J. Liu, E. M. J. Johansson, X. Zhang, *ACS Energy Lett.* **2021**, 6, 1970.
- [13] X. Zhang, Y. Justo, J. Maes, W. Walravens, J. Zhang, J. Liu, Z. Hens, E. M. J. Johansson, *J. Mater. Chem. A* **2015**, 3, 20579.
- [14] X. Zhang, C. Häggglund, E. M. J. Johansson, *Energy Environ. Sci.* **2017**, 10, 216.
- [15] X. Zhang, V. A. Öberg, J. Du, J. Liu, E. M. J. Johansson, *Energy Environ. Sci.* **2018**, 11, 354.
- [16] S. Zheng, J. Chen, E. M. J. Johansson, X. Zhang, *iScience* **2020**, 23, 101753.
- [17] D. C. J. Neo, N. Zhang, Y. Tazawa, H. Jiang, G. M. Hughes, C. R. M. Grovenor, H. E. Assender, A. A. R. Watt, *ACS Appl. Mater. Interfaces* **2016**, 8, 12101.
- [18] J. Yang, S. C. Cho, S. Lee, J. W. Yoon, W. H. Jeong, H. Song, J. T. Oh, S. G. Lim, S. Y. Bae, B. R. Lee, M. Ahmadi, E. H. Sargent, W. Yi, S. U. Lee, H. Choi, *ACS Nano* **2022**, 16, 1649.
- [19] M. Al Mubarak, H. Aqoma, F. T. A. Wibowo, W. Lee, H. M. Kim, D. Y. Ryu, J. W. Jeon, S. Y. Jang, *Adv. Energy Mater.* **2020**, 10, 1902933.
- [20] M. Al Mubarak, F. T. A. Wibowo, H. Aqoma, N. Vamsi Krishna, W. Lee, D. Y. Ryu, S. Cho, I. H. Jung, S. Y. Jang, *ACS Energy Lett.* **2020**, 5, 3452.
- [21] J. Liu, Y. Liu, J. Wang, H. Li, K. Zhou, R. Gui, K. Xian, Q. Qi, X. Yang, Y. Chen, W. Zhao, H. Yin, *Adv. Energy Mater.* **2022**, 2201975, <https://doi.org/10.1002/aenm.202201975>.
- [22] J. Liu, J. Qiao, K. Zhou, J. Wang, R. Gui, K. Xian, M. Gao, H. Yin, X. Hao, Z. Zhou, L. Ye, *Small* **2022**, 18, 2201387.
- [23] H. Il Kim, S. W. Baek, H. J. Cheon, S. U. Ryu, S. Lee, M. J. Choi, K. Choi, M. Biondi, S. Hoogland, F. P. G. de Arquer, S. K. Kwon, Y. H. Kim, T. Park, E. H. Sargent, *Adv. Mater.* **2020**, 32, 2004985.
- [24] S. W. Baek, S. Jun, B. Kim, A. H. Proppe, O. Ouellette, O. Voznyy, C. Kim, J. Kim, G. Walters, J. H. Song, S. Jeong, H. R. Byun, M. S. Jeong, S. Hoogland, F. P. García de Arquer, S. O. Kelley, J. Y. Lee, E. H. Sargent, *Nat. Energy* **2019**, 4, 969.
- [25] Y. Zhang, Y. Kan, K. Gao, M. Gu, Y. Shi, X. Zhang, Y. Xue, X. Zhang, Z. Liu, Y. Zhang, J. Yuan, W. Ma, A. K. Y. Jen, *ACS Energy Lett.* **2020**, 5, 2335.
- [26] H. Il Kim, J. Lee, M. J. Choi, S. U. Ryu, K. Choi, S. Lee, S. Hoogland, F. P. G. de Arquer, E. H. Sargent, T. Park, *Adv. Energy Mater.* **2020**, 10, 2002084.
- [27] Y. Liu, K. Xian, Z. Peng, M. Gao, Y. Shi, Y. Deng, Y. Geng, L. Ye, *J. Mater. Chem. A* **2021**, 9, 19874.
- [28] Y. Liu, K. Xian, X. Zhang, M. Gao, Y. Shi, K. Zhou, Y. Deng, J. Hou, Y. Geng, L. Ye, *Macromolecules* **2022**, 55, 3078.
- [29] Y. Liu, K. Xian, R. Gui, K. Zhou, J. Liu, M. Gao, W. Zhao, X. Jiao, Y. Deng, H. Yin, Y. Geng, L. Ye, *Macromolecules* **2022**, 55, 133.
- [30] M. Gao, Y. Liu, K. Xian, Z. Peng, K. Zhou, J. Liu, S. Li, F. Xie, W. Zhao, J. Zhang, X. Jiao, L. Ye, *Aggregate* **2022**, e190, <https://doi.org/10.1002/agt2.190>.
- [31] G. X. Jia, S. Q. Zhang, L. Yang, C. He, H. L. Fan, J. H. Hou, *Acta Phys-Chim. Sin.* **2019**, 35, 76.
- [32] F. Chen, Y. Zhang, Q. Wang, M. Gao, N. Kirby, Z. Peng, Y. Deng, M. Li, L. Ye, *Chinese J. Chem.* **2021**, 39, 2570.
- [33] K. Zhou, K. Xian, L. Ye, *InfoMat* **2022**, 4, e12270.
- [34] K. Xian, Y. Liu, J. Liu, J. Yu, Y. Xing, Z. Peng, K. Zhou, M. Gao, W. Zhao, G. Lu, J. Zhang, J. Hou, Y. Geng, L. Ye, *J. Mater. Chem. A* **2022**, 10, 3418.
- [35] H. Aqoma, M. Al Mubarak, W. Lee, W. T. Hadmojo, C. Park, T. K. Ahn, D. Y. Ryu, S. Y. Jang, *Adv. Energy Mater.* **2018**, 8, 1800572.
- [36] Y. Zhong, A. R. Kirmani, X. Lan, J. Carpenter, A. Chew, O. Awartani, L. Yu, M. R. Niazi, O. Voznyy, H. Hu, G. Ngongang Ndjawa, M. L. Tietze, A. Salleo, H. Ade, E. H. Sargent, A. Amassian, *J. Mater. Chem. A* **2022**, 10, 1788.
- [37] a) Y. Chen, H. Chen, H. Guan, W. Liu, Z. Li, H. Liu, Y. Li, Y. Zou, *Chinese Chem. Lett.* **2021**, 32, 229; b) F. Peng, K. An, W. K. Zhong, Z. Y. Li, L. Ying, N. Li, Z. Q. Huang, C. G. Zhu, B. B. Fan, F. Huang, Y. Cao, *ACS Energy Lett.* **2020**, 5, 3702.
- [38] C. Yang, S. Zhang, J. Ren, P. Bi, X. Yuan, J. Hou, *Chinese Chem. Lett.* **2021**, 32, 2274.
- [39] a) K. Zhou, K. Xian, Q. Qi, M. Gao, Z. Peng, J. Liu, Y. Liu, S. Li, Y. Zhang, Y. Geng, L. Ye, *Adv. Funct. Mater.* **2022**, 32, 2201781; b) Z. Peng, L. Ye, H. Ade, *Mater. Horiz.* **2022**, 9, 577.
- [40] Q. Qi, Y. Zhong, Y. Liu, M. Gao, Z. Peng, S. Li, W. Zhao, H. Ke, J. Zhang, L. Ye, *ACS Appl. Polym. Mater.* **2022**, 4, 1826.
- [41] L. Ye, M. Gao, J. Hou, *Sci. China Chem.* **2021**, 64, 1875.
- [42] Q. Wang, M. Li, Z. Peng, N. Kirby, Y. Deng, L. Ye, Y. Geng, *Sci. China Chem.* **2021**, 64, 478.
- [43] L. Ye, S. Li, X. Liu, S. Zhang, M. Ghasemi, Y. Xiong, J. Hou, H. Ade, *Joule* **2019**, 3, 443.
- [44] L. Ye, H. Hu, M. Ghasemi, T. Wang, B. A. Collins, J. H. Kim, K. Jiang, J. H. Carpenter, H. Li, Z. Li, T. McAfee, J. Zhao, X. Chen, J. L. Y. Lai, T. Ma, J. L. Bredas, H. Yan, H. Ade, *Nat. Mater.* **2018**, 17, 253.
- [45] L. Ye, H. Ke, Y. Liu, *Trends Chem.* **2021**, 3, 1074.
- [46] D. Jeong, G. Kim, D. Lee, S. Seo, S. Lee, D. Han, H. Park, B. Ma, S. Cho, B. J. Kim, *Adv. Energy Mater.* **2022**, 12, 2201603.
- [47] X. Yuan, Y. Zhao, D. Xie, L. Pan, X. Liu, C. Duan, F. Huang, Y. Cao, *Joule* **2022**, 6, 647.
- [48] K. Xian, Y. Geng, L. Ye, *Joule* **2022**, 6, 941.